A Full-Potential LMTO Method Based on Smooth Hankel Functions

M. Methfessel[1], M. van Schilfgaarde[2], and R. A. Casali[3]

[1] Institute for Semiconductor Physics, Walter-Korsing-Str. 2, D-15230 Frankfurt (Oder), Germany
[2] SRI International, 333 Ravenswood Avenue, Menlo Park, California 94025 (Present Address: Sandia National Laboratories, Livermore, California 94551)
[3] Department of Physics, Universidad Nacional del Nordeste, 3400 Corrientes, Argentina

Abstract. The paper presents a recently developed full-potential linear muffin-tin orbital (FP-LMTO) method which does not require empty spheres and can calculate the forces accurately. Similar to previous approaches, this method uses numerical integration to calculate the matrix elements for the interstitial potential, which is the limiting step for any FP-LMTO approach. However, in order to reduce the numerical effort as far as possible, we use a newly introduced basis consisting of "augmented smooth Hankel functions" which play the role of the LMTO envelope functions. After presenting the basics of the approach, we report the results of numerical test for typical condensed-matter systems. The calculations show that good accuracy can be reached with an almost minimal basis set. These features of the method open the way to efficient molecular dynamics studies and simulated-annealing calculations to optimize structures while retaining the advantages of the LMTO method.

1 Introduction

The linear muffin-tin orbital (LMTO) method [1] has played a very successful role among the various techniques for solving the density-functional equations [2] for a condensed-matter system. Two characteristic features of this approach are (i) the use of atom-centered basis functions of well-defined angular momentum, constructed out of Hankel functions, and (ii) the use of augmentation to introduce atomic detail into the basis functions in the vicinity of each nucleus. Overall, the rationale behind this approach is to construct basis functions which closely resemble the actual wavefunctions from the very beginning. The consequence is that a comparatively small basis set already leads to a converged total energy, hopefully giving rise to substantial reductions in the computation time and the storage requirements.

In general term, when using a sophisticated basis in this manner, it is not *a priori* clear that these savings will actually be the realized. The price for a more sophisticated basis set is an increased computational effort in some steps of the calculation. This extra effort may or may not cancel out the gain due to the reduced basis size. For the LMTO method, the balance is no doubt positive if the atomic-sphere approximation (ASA) [3] is used. Hereby the single-electron

H. Dreyssé (Ed.): Workshop 1998, LNP 535, pp. 114–147, 1999.

potential is modeled by a superposition of spherical potentials inside overlapping space-filling spheres. Where this approximation is applicable, the LMTO-ASA method is presumably the most efficient procedure available for solving the density-functional equations to a reasonably high degree of accuracy. However, a "full-potential" treatment which goes beyond the ASA is needed for many systems of interest. Typical examples are the total energy changes associated with phonons distortions and atomic relaxations, say at a surface or around an impurity. Furthermore, for low-symmetry situations the LMTO-ASA method becomes unwieldy as the question of "empty spheres" to improve the packing fraction becomes more important. Finally, since the energies associated with such distortions are not reliable, the question of the calculation of the forces on the atoms does not even arise. However, the forces are precondition for simulated annealing and molecular dynamics studies in the spirit of the Car-Parrinello [4] method.

A number of different approaches have been developed in the past to go beyond the ASA in the LMTO method. Their common element is that the potential is treated correctly within the existing LMTO basis set. Unfortunately, this has lead to a substantial increase in the computational effort. In the interest of efficiency, we have explored and implemented a novel approach in which the LMTO basis functions themselves are modified in a controlled manner. This has two benefits: the basis set can be even smaller, and the effort for a numerical integration of the potential matrix elements is reduced. At the same time, a reformulation of the augmentation procedure is required since the standard structure-constant expansion cannot be used for the modified functions. Turning this into an advantage, we have used a "projection" description which is partly based on previous developments due to Blöchl [5] and Vanderbilt [6] but which includes some new features. Among other benefits, the separation into a "smooth" and atomic "local" terms is cleaner, leading to a straightforward expression for the forces.

Overall, the following criteria were considered imperative when developing this variant of the LMTO method:

- The forces must be calculated.
- All reasonable geometries should be handled without the need for empty spheres.
- It must be possible to improve the accuracy systematically by turning up the various convergence parameters.

Within these requirements, it was tried as far as possible to maintain the characteristic advantages of computational efficiency and small memory demands.

In the rest of this paper, the modified LMTO envelope functions are discussed in Sect. 2.2. The reformulated augmentation procedure and the force theorem are described in Section 2.3. Finally, we present some practical experience with the resulting method in Section 3. Specifically, we investigate the dependence of the results on the various convergence parameters and compare to calculations with other methods for a number of realistic systems.

2 Description of the Method

This section presents the basic ideas behind the method. After a discussion the central role of the interstitial potential matrix elements, the modified LMTO-like envelope functions (smooth Hankel functions) are presented. Finally, the reformulated augmentation procedure and the forces are discussed.

2.1 The Central Role of the Interstitial Potential Integrals

In a density-functional calculation, the three main tasks are (i) to solve the Poisson equation and to add on the exchange-correlation potential, making the effective potential felt by an electron, (ii) to solve the single-particle Schrödinger equation, and (iii) to add together the squared moduli of the wavefunctions to accumulate the new output density. In most cases, the solution of Schrödinger's equation is the most difficult and the most expensive step of these. In fact, if the potential is to be treated without any further approximation (*i.e.*, in a "full-potential" method), the main bottlenecks usually turn out to be in two closely related substeps:

- To set up the Hamiltonian matrix, we require the matrix elements of the effective potential $V_{\text{eff}}(\boldsymbol{r})$ for the basis functions $\chi_i(\boldsymbol{r})$:

$$V_{ij} = \int \chi_i^*(\boldsymbol{r}) V_{\text{eff}}(\boldsymbol{r}) \chi_j(\boldsymbol{r})\, d\boldsymbol{r} \ . \tag{1}$$

- To obtain the output density, we must sum over the squared moduli of the wave functions $\psi_n(\boldsymbol{r})$:

$$n^{\text{out}}(\boldsymbol{r}) = \sum_{n\text{occ}} w_n \left|\psi_n(\boldsymbol{r})\right|^2 \ . \tag{2}$$

Since the wavefunction is a linear combination of the basis functions, the real task when making the output density is to express the product of any two basis functions $\chi_i^* \chi_j$ in a form suitable for further handling. Specifically, we must be able to evaluate the integral of this product times the potential, since this is one important contribution in the total energy. Furthermore, the representation must "close the loop" so that the output density can be mixed with the input density and the result fed into the next iteration. In practice, both of the steps above are essentially the same problem, namely the evaluation of the potential integrals of (1).

In augmentation approaches such as the LMTO and linear augmented plane-wave (LAPW) methods [1], space is partitioned into atom-centered muffin-tin spheres and an interstitial region. The potential integrals split up accordingly into the integrals over the two types of region. The contributions from the muffin-tin spheres can be calculates in a straightforward and reasonably efficient manner since the potential as well as the basis functions can be expressed using one-center expansions. That is, each function is written in polar coordinates around the relevant sphere center as a radial part times a spherical harmonic.

Thus, the term which requires most attention is in fact only the interstitial contribution to the potential matrix element:

$$V_{ij}^{(\mathrm{IR})} = \int_{\mathrm{IR}} H_i^*(\boldsymbol{r}) V(\boldsymbol{r}) H_j(\boldsymbol{r})\, d\boldsymbol{r} \ . \tag{3}$$

Here the functions $H_i(\boldsymbol{r})$ denote the envelope functions, *i.e.*, the analytic functions which will be augmented inside the atomic spheres to obtain the final basis functions $\chi_i(\boldsymbol{r})$, and IR denotes the interstitial region. This matrix element is always problematic, independent of the representation chosen for the interstitial potential. In fact, a major part of devising a viable method is to select a representation for the density and the potential which makes it possible to compute these matrix elements reasonably efficiently. The efficiency of the LMTO-ASA method is clear: by making the atomic spheres space filling and neglecting the interstitial potential, the most demanding computational step is eliminated, leaving only terms which can be evaluated in a compact and effective manner.

Basically there are two ways to proceed in a full-potential approach. First, the potential in the interstitial region can be expanded in some suitable set of auxiliary functions. For example, a set of atom-centered functions can be used, which can lead to a very compact representation. Substituting the expansion under the integral in (3) leads to a sum of integrals, each over a product of three terms. Unfortunately, such integrals can almost never be evaluated in closed form (the notable exception is when all terms are gaussians). In our context, two of the terms are LMTO envelopes, and no reasonable choice of a potential expansion considered to date leads to a closed form.

Alternatively, the interstitial potential can be specified by tabulating it on a regular mesh which extends through the unit cell. Equivalently, the coefficients of the Fourier expansion of the potential can be given. Although such a numerical representation requires more data to specify the potential, there are some considerable advantages. First, since the exchange-correlation potential must be evaluated point by point, a mesh representation is needed at some stage in any case. Second, by using a regular mesh the Poisson equation can be solved easily using a fast Fourier transform. Third, the additional step of fitting the output density or the effective potential to the set of auxiliary functions is avoided. Finally, enhancements such as gradient corrections can be implemented more easily on a regular mesh than in a more complicated representation. For these reasons, a real-space mesh representation of the interstitial potential (as well as the interstitial density) will be used in the following. In effect, we have opted for a hybrid treatment in which the wavefunctions are represented using a carefully constructed atom-centered basis set but the interstitial potential and density are given as numerical tabulations.

At this point, a comparison to different existing methods is in order. The generally used procedure is to extend the basis functions and the interstitial potential smoothly through the atomic spheres in some manner, to integrate (3) over the complete unit cell using these smooth functions, and finally to subtract off the unwanted contributions inside the spheres in conjunction with the augmentation step. In the full-potential LAPW method, all the involved functions

are simply plane waves and the integral over the cell can be written down immediately. In the various FP-LMTO approaches, the smooth extension must be explicitly constructed for the sphere on which the function is the centered. This can be done by matching an analytical expression (such as a polynomial) at the sphere radius [7,8] or by using analytical functions similar to ours with a suitable choice of the parameters [9]. In either case, care must be taken that the resulting function strictly equals the standard LMTO envelope in the interstitial region. The alternative approach followed in this paper is to "bend over" the envelope functions already in the interstitial. As discussed next, this reduces the basis size and at the same time permits a coarser mesh for the numerical integration. We note that a completely different approach to the interstitial potential matrix elements is to re-expand the product of any two envelopes as a sum of auxiliary atom-centered basis functions. In this way the integrals over three factors in (3) are changed to a sum of two-center integrals. The expansion can be obtained approximately by fitting on the surfaces of the muffin-tin spheres [10] or more accurately for molecules by tabulating the results of a careful numerical fit [11]. Furthermore, an approach suitable for molecules and polymers has been developed which handles integrals over the product of three Hankel functions by expanding two of the terms around the site of the third [12].

2.2 Smooth Hankel Functions

In the following, we present the advantages of an LMTO-like basis consisting of augmented smoothed Hankel functions. The standard LMTO envelope function is a Hankel function of a (usually) zero or negative energy parameter times a spherical harmonic. This object will be denoted as a "solid Hankel function" in the following. It solves the Schrödinger equation for a flat potential, decays exponentially at large distances if the energy parameter is negative, and has a singularity at the site where it is centered. The essence of our modification is to remove the singularity. The resulting "smooth Hankel function" is smooth and analytic in all parts of space. When such a function is used to construct the basis, the parameters can (and should) be chosen so that the functions deviate from the unsmoothed variants already outside the central atomic sphere. As will be explained below, this speeds up the calculation for two separate reasons: the basis can be smaller, and numerical integration can be done using a coarser mesh.

Basic Properties

The smooth Hankel functions (discussed in detail in Refs. [13,14]) are shown in Fig. 1 for angular momentum 0, 1, and 2. For large radii, the smooth function to each angular momentum equals the corresponding standard Hankel function, showing the same exponential decay proportional to $\exp(-\kappa r)$, as specified by the negative energy parameter $\epsilon = -\kappa^2$. At smaller radii, the function bends over gradually until it finally approaches r^l close to $r = 0$. When multiplied by the spherical harmonic $Y_L(\hat{r})$, the result is analytic in all parts of space.

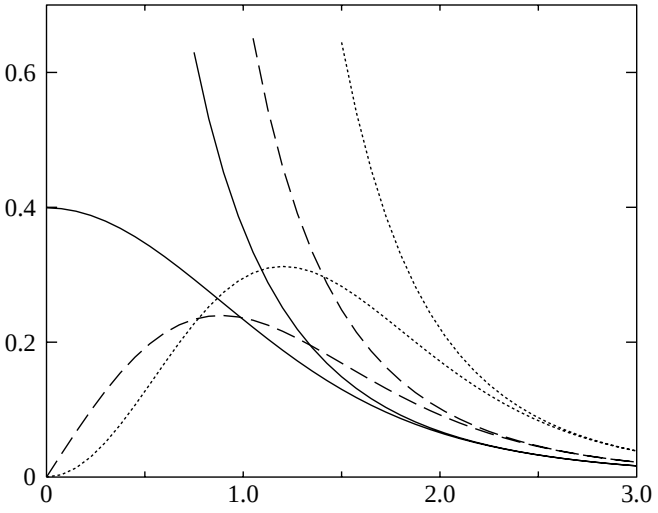

Fig. 1. Comparison of smooth and standard Hankel functions for l=0 (continuous lines), l=1 (dashed), and l=2 (dotted lines). The energy ϵ equals -1 and the smoothing radius $R_{\rm sm}$ equals 1.0. For large radii, the smooth and standard functions coincide. Near the origin, the smooth function bends over gradually until it enters as r^l whereas the standard function has a singularity proportional to $1/r^{l+1}$.

Of some importance is the parameter $R_{\rm sm}$, denoted as the "smoothing radius" associated with the function. For practical purposes, the standard Hankel function and its smooth variant are equal where the gaussian $\exp(-r^2/R_{\rm sm}^2)$ is negligible, say for $r > 3R_{\rm sm}$ When $R_{\rm sm}$ is increased, the deviation from the standard function starts at a larger value of r and the resulting function is more strongly smoothed. Specifically, the value at $r = 0$ for $\ell = 0$ becomes smaller as the former singularity is washed out more and more.

A central distinction to the standard LMTO envelopes is that two separate parameters determine the shape of each function. More exactly, the energy parameter determines the exponential decay at large radii, and the smoothing radius determines how strongly the function has been smoothed. Consequently, in order to tune the function to mimic the true wavefunction as far as possible, both of these parameters should be adjusted.

As a basis set, these functions combine many of the advantages of Hankel functions and gaussians. In fact, a smooth Hankel function is a convolution of these two types of functions. Due to the exponential decay at large radii, they constitute a numerically more stable and more compact basis than pure gaussians. In contrast to the standard Hankel functions, they have a smooth nonsingular shape near the origin. Furthermore, many important quantities (such as two-center integrals) can be evaluated analytically.

Formally, the smooth Hankel functions are defined in the following way. The usual Hankel function for angular momentum zero is $h_0(r) = e^{-\kappa r}/r$ where κ

defines the decay at large radii. As a function of $r = |\boldsymbol{r}|$ in three-dimensional space, h_0 satisfies the differential equation

$$(\Delta + \epsilon)h_0(r) = -4\pi\delta(\boldsymbol{r}) \tag{4}$$

where $\epsilon = -\kappa^2$ is the energy associated with the function, here always taken to be negative. Thus, $\Delta + \epsilon$ applied to h_0 is zero everywhere except at $\boldsymbol{r} = 0$, where a delta function arises from the $1/r$ singularity of h_0. Expressed differently, $h_0(r)$ is the response of the operator $\Delta + \epsilon$ to a delta-function source term.

To change this standard Hankel function into a "smooth Hankel function" the infinitely sharp delta function is smeared out into a gaussian:

$$(\Delta + \epsilon)h_0(r) = -4\pi g_o(r) \ . \tag{5}$$

By defining a suitable normalization of the modified source term $g_0(r) = C\exp(-r^2\ /R_{\mathrm{sm}}^2)$, the smooth Hankel approaches the standard function for large r. As r becomes smaller and reaches the range where $g_0(r)$ is non-negligible, the function $h_0(r)$ now bends over smoothly and behaves as a constant times r^l for $r \to 0$.

We will also need smooth Hankel functions for higher angular momenta in order to construct basis functions for the s, p, d... states. These can be constructed by applying the differential operator $\mathcal{Y}_L(-\nabla)$ defined as follows. The spheric harmonic polynomial $\mathcal{Y}(\boldsymbol{r}) = r^l Y_L$ is a polynomial in x, y, and z, for example $C(x^2 - y^2)$. By substituting the partial derivatives $-\partial_x$, $-\partial_y$, and $-\partial_z$ for x, y, and z, respectively, the required operator is obtained in a straightforward manner. Applying this operator to the delta function yields point dipoles, quadrupoles and so on, and applying it to $g_0(r)$ yields smeared-out gaussian versions of these. Thus the L-th smooth Hankel functions is $H_L(\boldsymbol{r}) = \mathcal{Y}_L(-\nabla)h_0(r)$ and satisfies the differential equation

$$(\Delta + \epsilon)H_L = -4\pi G_L(\boldsymbol{r}) = -4\pi\mathcal{Y}_L(-\nabla)g_0(r) \ . \tag{6}$$

A number of important quantities can be calculated analytically for these functions, including the overlap integral and the kinetic energy expectation value between any two functions. They can also be expanded around some point in the unit cell. For further details, see Ref. [14].

Advantages of Smooth-Hankel Envelopes

The first reason for using the smooth-Hankel basis functions is that this reduces the size of the basis set, leading to a substantial gain in efficiency. To make this plausible, note that the standard LMTO basis functions are in fact not optimal as a basis for representing the crystal or molecular wave functions. The main problem is that they are "too steep" in the interstitial region close to the muffin-tin sphere on which they are centered. This is illustrated in Fig. 2. The standard Hankel functions solves Schrödinger's equation for a flat potential. However, when approaching a nucleus the true crystal potential is not flat

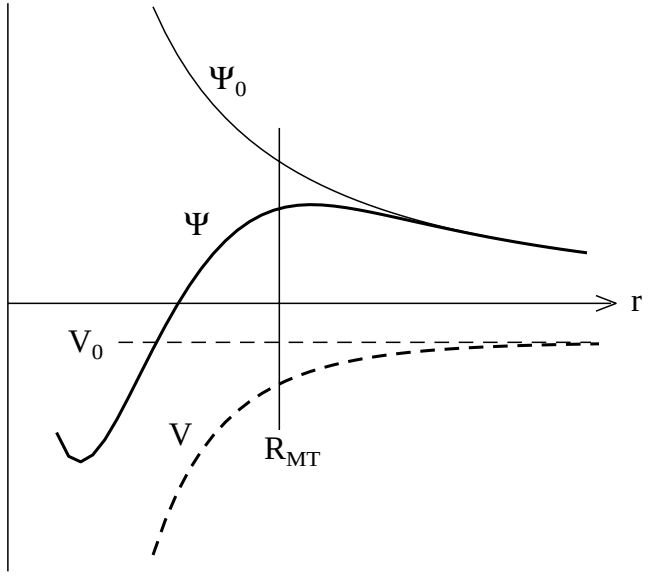

Fig. 2. Sketch to explain why smooth Hankel functions lead to an improved basis. For the flat potential V_0, the solution of the radial Schrödinger equation Ψ_0 is a standard Hankel function with a singularity at the origin. As the true potential V starts to feel the attractive nuclear potential, the correct wavefunction Ψ bends over. This behavior already starts outside the muffin-tin radius and is built into the smooth Hankel functions.

but decreases as it feels the attractive nuclear potential. The curvature of the wavefunction equals the potential minus the energy which therefore becomes negative. In response, the wavefunction bends over and changes from exponential to oscillatory behavior. By using smooth Hankel functions, this typical form is inherent in each basis function.

This effect can be appreciated by inspecting the way in which the standard LMTO basis functions combine to describe a crystal wavefunction. Generally the basis set must include some slowly decaying functions together with others which are considerably more localized. In the course of the calculation these combine with opposite signs, in this way modeling the required change of curvature. Using smooth Hankel functions as envelopes, these already have the correct behavior and some of the additional localized functions can be left away.

In practice, the amount of gain depends on the type of atom. For the important angular momenta, a tripled basis can often be replaced by a doubled set. Less important channels such as the d states in an sp atom can be described by one radial function instead of two. An overall reduction by a factor of almost two is sometimes possible. In the order(N^3) steps, the computation time in such a favorable case divides by eight.

The second major advantage to using smooth Hankel functions instead of the standard LMTO envelopes is that the time-consuming matrix elements (3) for the interstitial potential can be calculated more efficiently. As described above, the integrals can be obtained by integrating over the complete unit cell using a regular mesh and subsequently subtracting the contributions inside the spheres. The danger when calculating three-dimensional integrals using a mesh is that the computational effort can easily dominate all other steps. To keep the effort manageable, it is of high priority to make the integrands as smooth as possible. This can be done by using smooth Hankels as envelopes. As an example, consider silicon with a muffin-tin radius of 2.2 bohr. For the standard LMTO basis, the smoothing must be noticeable inside the MT sphere only, demanding a smoothing radius no larger than 0.6 to 0.7 bohr. Outside the central sphere, the smooth and conventional Hankel functions are then identical to acceptable precision. The required integration mesh spacing is approximately 0.35 bohr. If we permit the functions to bend over outside the MT sphere, we find that the optimal basis functions have a smoothing radius of about 1.4 bohr. For these functions, the integration mesh can be twice as coarse. Consequently the number of mesh points and the computational effort are divided by eight.

At this point it should already be mentioned that in the final implementation, the matrix elements of the smooth potential are actually calculated in reciprocal space. While this is at first sight equivalent to a real-space integration, the important difference is that a different reciprocal-space cutoff can be used for each function. For integrals involving envelopes with a large smoothing radius, a small cutoff is adequate. This property is very important for systems such as an oxygen impurity in silicon. The O basis functions demand a fine underlying real-space mesh through the unit cell, but this is effectively only used for the O functions. The effort for integrals between Si functions can be calculated with the same effort as without the presence of the oxygen atom.

Altogether, a modified basis using "smooth Hankel functions" combines two major advantages. Since these are more similar to the final wavefunctions, adequate convergence can be attained using a smaller basis set. Secondly, since each function is smoother, the mesh used to evaluate the potential integral can be coarser. These effects combine to a substantial saving in computer time. As an estimate (admittedly for an extremely favorable case), the integration mesh can be twice as coarse, leading to a saving of about $(1/2)^3 = 1/8$ in the order-3 steps. The basis set will contain something like one-half of the functions needed without extra smoothing, giving another factor of approximately 1/8. Together, the computer time is divided by 64. While the overall gain will not be as large for many systems, a speedup by a factor between 10 to 20 is realistic.

Analytical Two-Center Integrals

In the preceding, it was explained how the smooth Hankel functions help to evaluate the matrix elements of the interstitial potential more efficiently. In the course of a calculation, we also require the matrix elements of the kinetic energy operator and the overlap integrals. A major advantage of the smooth Hankel

functions is that these integrals can be evaluated analytically. In fact, most two-center integrals involving these functions as well as gaussians can be obtained in basically the same way. The idea is to use Parseval's equality:

$$\int f_1(\boldsymbol{r})^* f_2(\boldsymbol{r})\, d\boldsymbol{r} = \frac{1}{(2\pi)^3} \int \hat{f}_1^*(\boldsymbol{q}) \hat{f}_2(\boldsymbol{q})\, d\boldsymbol{q} \tag{7}$$

and the explicit expression for the Fourier transform of a smooth Hankel function $H_L(\boldsymbol{r})$ located at some site $\boldsymbol{R}$:

$$\hat{H}_L(\boldsymbol{q}) = \frac{-4\pi}{\epsilon - q^2} e^{\gamma(\epsilon - q^2)} \mathcal{Y}_L(-\mathrm{i}\boldsymbol{q}) e^{-\mathrm{i}\boldsymbol{q}\cdot\boldsymbol{R}} \tag{8}$$

where $\gamma = R_{\mathrm{sm}}^2/4$ is one-fourth of the squared smoothing radius. When two such expressions are multiplied together, the result can be readily written as a sum of terms of the same basic form, combined with additional powers of q^2 arising from the Clebsch-Gordon factorization of $\mathcal{Y}_L(-\mathrm{i}\boldsymbol{q})^* \mathcal{Y}_{L'}(-\mathrm{i}\boldsymbol{q})$. Since the phase factor in the product is $\exp[\mathrm{i}\boldsymbol{q}\cdot(\boldsymbol{R}_1 - \boldsymbol{R}_2)]$, the final result is that the desired integral can be expressed analytically as a sum of smooth Hankel functions, evaluated for the connecting vector between the two sites. Hereby the extra powers of q^2 mean that the (only slightly more complicated) functions ΔH_L, $\Delta^2 H_L$ ... are also needed. Furthermore, the resulting expression for the two-center integral is equally valid for molecular and Bloch-summed functions. In the later case, the only difference is that Bloch functions are also substituted in the final analytical expression. In addition to the overlap integrals considered here, integrals involving any power of the kinetic energy operator $-\Delta$ as well as Coulomb integrals can be calculated analytically in a similar manner. Another related application is to obtain the coefficients of a local expansion around another site, as described next.

Expansion Around a Site

In order to do perform the augmentation in practice, one of the steps which is needed is to expand a smooth Hankel function around some point in the unit cell. Far away from the center, the smooth Hankel function equals the unsmooth variant and the well-known structure constant expansion for the standard Hankel functions could be used. On the central sphere, the function is given explicitly by its definition. It is for sites close to the central sphere, such as nearest-neighbor atoms, where something new is needed. Here the function generally starts to bend over and the standard expansion does not apply.

This problem is solved as follows. We define a family of higher-order gaussians $G_{kL}(\boldsymbol{r})$ by applying differential operators to the seed function $g_0(r) = C\exp(-r^2/R_{\mathrm{sm}}^2)$:

$$G_{kL}(\boldsymbol{r}) = \Delta^k \mathcal{Y}_L(-\nabla) g_0(r)\ . \tag{9}$$

We can construct biorthogonal polynomials to these functions, *i.e.*, a set of polynomials $P_{kL}(\boldsymbol{r})$ with the property

$$\int G_{kL}(\boldsymbol{r}) P_{k'L'}(\boldsymbol{r})\, d\boldsymbol{r} = \delta_{kk'}\delta_{LL'}\ . \tag{10}$$

In fact, it turns out that P_{kL} is just G_{kL} divided by $g_0(r)$ times a normalization constant. To expand an arbitrary function $f(\boldsymbol{r})$ as a sum of the P_{kL}, each coefficient can be calculated by the integral over $f(\boldsymbol{r})$ times the corresponding gaussian:

$$f(\boldsymbol{r}) = \sum_{kL} A_{kL} P_{kL}(\boldsymbol{r}) \tag{11}$$

where

$$A_{k_L} = \int f(\boldsymbol{r}) G_{kL}(\boldsymbol{r})\, d\boldsymbol{r} \ . \tag{12}$$

This expansion, when truncated to some low value of k, is considerably more accurate than, for example, a Taylor series. This is because the expansion converges smoothly towards $f(\boldsymbol{r})$ in the range where $g_0(r)$ is large as more terms are included. When $f(\boldsymbol{r})$ is a smooth Hankel function centered anywhere in space, the integrals defining expansion coefficients can be done analytically. This supplies the desired local expansion.

The expansion is used in several different steps, most prominently to augment the envelope functions. Note that in this procedure, there are two distinct parameters which influence the accuracy of the expansion. By choosing a cutoff $p_{\max}$ for the terms in the expansion, the radial function is represented as a polynomial of order $p_{\max}$. The range over which the expansion is accurate is determined by the smoothing radius R_{sm} of the projection gaussians G_{kL}. When R_{sm} is chosen larger, the expansion can be used over a larger part of space but will not be as accurate overall for the same value of $p_{\max}$. Choosing R_{sm} in the vicinity of one-third of the muffin-tin radius will usually give a reasonable expansion within the muffin-tin sphere.

2.3 Augmentation

In the following, we describe the modified augmentation procedure used in the method. In general terms, the pseudopotential formulation and augmentation are two competing approaches to introduce atomic detail into the wavefunction near the nuclei. When a pseudopotential formulation is used, this is implicit: although only smooth functions are manipulated during a calculation, the true wavefunctions could be derived from these in a well-defined manner. When augmentation is used, the basis functions are explicitly constructed to show the required strongly-varying and oscillatory character close to an atom. The first step is to cut space into atomic spheres and an interstitial region. Throughout the interstitial region, the basis functions are equal to suitable smooth "envelope functions" which in the present case are the smooth Hankel functions introduced above. Inside each atomic sphere, every envelope function is replaced by a numerical solution of the Schrödinger equation. Specifically, in the well-known linear methods [1], numerical solutions of the Schrödinger equation in the spheridized potential and their energy derivatives are combined to match smoothly to the

envelope function at the sphere boundary. Overall, this procedure amounts to a piecewise definition of the basis function in different parts of space.

Comparing the two approaches, the norm-conserving pseudopotential formulation [15] has a number of advantages, once the initial effort of constructing the pseudopotential has been completed. Angular momentum cutoffs are generally low and an expression for the force is easy to obtain. In contrast, since augmentation works by cutting out the part of space near the nucleus and treating it separately, quantities must sometimes be expanded to relatively high angular momenta. Due to the complexity of the augmentation procedure, it is often difficult to derive a valid force theorem. In practice, the augmentation and pseudopotential approaches have some similarity. Both methods expand a set of smooth basis functions by angular momentum around the different sites, then operate on the different angular momentum components independently. This suggests that a more unified description should be possible.

With the aim of a practical formulation for all-electron methods which has the simplicity and transferability of the pseudopotential approach, the formulation of augmentation described in the following shares some aspects with the projector augmented-wave (PAW) method [5] and has some similarity with Vanderbilt's ultrasmooth pseudopotentials [6]. As in the PAW method, "additive augmentation" is used to reduce angular-momentum cutoffs for the representation of the wavefunctions, charge density, and potential. However, the present approach eliminates the need to construct pseudopartial waves and projector functions. Also, completeness of the partial-wave expansion is not an issue, the force theorem here seems to be simpler, and orthogonality to the core states is automatic.

Augmented Basis Functions

As will be described in more detail below, the crystal potential will be written in the following form:

$$V(\boldsymbol{r}) = \tilde{V}_0(\boldsymbol{r}) + \sum_{\nu} \Big\{ V_{1\nu}(\boldsymbol{r}) - \tilde{V}_{2\nu}(\boldsymbol{r}) \Big\} \tag{13}$$

Here $\tilde{V}_0$ is a smooth potential extending through the unit cell, tabulated on a real-space mesh; $V_{1\nu}$ is the true potential inside the atomic sphere ν, given as an expansion in spherical harmonics times numerical radial functions, and $\tilde{V}_{2\nu}$ is the smooth mesh potential expanded in the same way. The tilde over a potential term indicates that compensating charges modeled by gaussians entered into the electrostatic contribution. One sees that the potential is expressed as a smooth function $\tilde{V}_0$ which is augmented by adding a local term $V_{1\nu} - \tilde{V}_{2\nu}$ inside each sphere. The relevant point is that the local expansions of $V_{1\nu}$ and $\tilde{V}_{2\nu}$ can be truncated at the (same) low angular-momentum cutoff l_{L} with small loss of accuracy. To obtain a smooth overall potential, $V_{1\nu}$ and $\tilde{V}_{2\nu}$ should have the same values and slopes at the sphere surface. The higher l-components of the two functions are closely similar and can be left away in the difference $V_{1\nu} - \tilde{V}_{2\nu}$.

This does not mean that the higher angular momentum components are set to zero in the total potential; instead, they are carried by the smooth mesh potential $\tilde{V}_0$.

After identifying the form in which the potential is specified, the next step is to calculate the Hamiltonian and overlap matrix elements for the basis functions $\chi_i(\boldsymbol{r})$, obtained by augmenting the (as yet unspecified) smooth envelope functions $F_i(\boldsymbol{r})$. The required integrals over the unit cell are

$$H_{ij} = \int \chi_i^*(\boldsymbol{r})[-\Delta + V(\boldsymbol{r})]\chi_j(\boldsymbol{r})\, d\boldsymbol{r} \tag{14}$$

$$S_{ij} = \int \chi_i^*(\boldsymbol{r})\chi_j(\boldsymbol{r})\, d\boldsymbol{r} \ . \tag{15}$$

At this stage, the envelopes could be the smooth Hankel functions, plane waves, or some other set of smooth functions extending through the unit cell.

In order to perform the augmentation, the first step is to project out local information about the envelopes near a chosen site. This can be done using some local set of radial functions, denoted by P_{kL}, used to expand the i-th envelope as

$$F_i(\boldsymbol{r}) = \sum_{kL} C_{kL}^{(i)} P_{kL}(\boldsymbol{r}) \ . \tag{16}$$

The notation anticipates that we will later use the polynomials of Section 2.2, but in this context the P_{kL} are general functions with well-defined angular momentum and sufficient radial degrees of freedom.

To augment, we first construct functions $\tilde{P}_{kL}$ which are augmented versions of the separate P_{kL}. Assuming P_{kL} is given in the form

$$P_{kL}(\boldsymbol{r}) = p_{kl}(r) Y_L(\hat{r}) \tag{17}$$

then the augmented version is defined as

$$\tilde{P}_{kL}(\boldsymbol{r}) = \tilde{p}_{kl}(r) Y_L(\hat{r}) = \Big[A_{kl}\phi_l(r) + B_{kl}\dot{\phi}_l(r) \Big] Y_L(\hat{r}) \tag{18}$$

where $\tilde{p}_{kl}(r)$ equals the contents of the square brackets. In the standard way, $\phi_l(r)$ and $\dot{\phi}_l(r)$ are a specific solution of the radial Schrödinger equation and its energy derivative, respectively. The coefficients A_{kl} and B_{kl} are chosen so that $\tilde{p}_{kl}$ and p_{kl} have the same value and derivative at the muffin-tin radius R_{mt}. The augmented envelope function then is

$$\tilde{F}_i(\boldsymbol{r}) = F_i(\boldsymbol{r}) + \sum_{kL} C_{kL}^{(i)} \Big\{ \tilde{P}_{kL}(\boldsymbol{r}) - P_{kL}(\boldsymbol{r}) \Big\} \ . \tag{19}$$

At first sight, this expression seems slightly nonsensical. Using (16), the first term should cancel against the last, leaving only a sum over the $\tilde{P}_{kL}$. The relevant feature is that, when the sums over k and L are truncated (as will be assumed from here on), the result is still close to the complete sum. Exactly as in the case of the potential, we start with a smooth function containing all components up to infinity and replace only a few of the lower terms by numerical functions.

Overlap and Kinetic Energy Matrix Elements

The next task is to calculate overlap integrals for the augmented envelope functions. These integrals are expressed as follows:

$$\int \tilde{F}_i^* \tilde{F}_j \, d\boldsymbol{r} = \int F_i^* F_j \, d\boldsymbol{r} + \sum_{kk'L} C_{kL}^{(i)*} \sigma_{kk'l} C_{k'L}^{(j)} \tag{20}$$

where

$$\sigma_{kk'l} = \int_S \left\{ \tilde{P}_{kL} \tilde{P}_{k'L} - P_{kL} P_{k'L} \right\} d\boldsymbol{r} \tag{21}$$

is an integral over the atomic sphere. For simplicity in the notation, it was assumed that there is one atom in the unit cell and that P_{kL} is real. Note that $\sigma_{kk'l}$ depends only on l, not on $L{=}(l,m)$. In (20), the integral is evaluated by first calculating the overlap between the smooth envelopes as an integral over the whole unit cell. Then local information about the envelopes is projected out in the form of the coefficient vectors $C^{(i)}$ and $C^{(j)}$. Finally, the product $C^{(i)\dagger}\sigma C^{(j)}$ is added, where σ is a small symmetric matrix characterizing the atom at this site.

It should be pointed out that equation (20) is not formally equal to the integral over $\tilde{F}_i^* \tilde{F}_j$ when these functions are given by (19). Instead, the straightforward integral over the product would lead to a large number of unwieldy cross terms. The point is that (20) gives the correct result when all sums are taken to infinity. For finite cutoffs, the result is a good approximation to that which would be obtained if no truncation were done. As before, this follows because the discarded terms in the integrals over $\tilde{P}_{kL}\tilde{P}_{k'L}$ and $P_{kL}P_{k'L}$ are similar. Therefore the truncation errors cancel to a large extent when the the difference between the two contributions to σ is taken. Thus, the question of leaving away the cross terms in the expression for this and similar matrix elements is purely a convergence issue: we have an expression which is correct when all terms to infinity are included, but which must be truncated to a suitable finite sum for a practical calculation. Consequently it is of high priority to arrange matters for rapid convergence.

As a second comment, let us assume for a moment that the radial augmentation functions ϕ_l and $\dot{\phi}_l$ are kept frozen throughout the calculation. This is usually a reasonable procedure in practice, although it was not done in the calculations presented further on. Then the augmented expansion functions $\tilde{P}_{kL}$ are also invariant and consequently the local matrix $\sigma_{kk'l}$ is completely independent of the environment. The formulation thus begins to approach that of a unique and transferable pseudopotential.

Analogous to the overlap integral, the kinetic energy integrals are given as follows:

$$\int \tilde{F}_i^* [-\Delta] \tilde{F}_j \, d\boldsymbol{r} = \int F_i^* [-\Delta] F_j \, d\boldsymbol{r} + \sum_{kk'L} C_{kL}^{(i)*} \tau_{kk'l} C_{k'L}^{(j)} \tag{22}$$

where

$$\tau_{kk'l} = \int_S \left\{ \tilde{P}_{kL}[-\Delta]\tilde{P}_{k'L} - P_{kL}[-\Delta]P_{k'L} \right\} d\boldsymbol{r} \ . \tag{23}$$

Although it is not immediately apparent, the local kinetic energy matrix $\tau_{kk'l}$ is also symmetric. When the operator $-\Delta$ is moved from the second to the first function under each integral, two surface terms over the sphere boundary arise. These cancel because $\tilde{P}_{kL}$ and P_{kL} match in value and slope. As in the case of the overlap, $\tau_{kk'l}$ is independent of the environment if the radial augmentation functions ϕ_l and $\dot{\phi}_l$ are kept frozen during the calculation.

Potential Matrix Elements

The potential matrix element is somewhat more complicated. The electrostatic potential inside a given sphere depends not only on the density inside this sphere, but also on the density in all other parts of the unit cell. This is one reason why it is not easy to separate out a transferable local potential from the overall eigenvalue problem, even though this is a fundamental feature of the pseudopotential approach.

In precise terms, the potential is an auxiliary function needed to minimize the total energy respective to the trial density. Taken times some density variation and integrated, the potential should give the first-order response of the electrostatic and exchange-correlation energy for the given variation of the trial density. As described below, when evaluating the electrostatic energy, compensating gaussians are added to the smooth mesh density to make a "pseudodensity" with the correct multipole moments in the spheres. This construction enters into the total energy and, as a consequence, gives rise to certain terms in the potential matrix elements. To formulate this properly, write the total crystal density in a way similar to the potential (13) as

$$n(\boldsymbol{r}) = n_0(\boldsymbol{r}) + \left\{ \rho_1(\boldsymbol{r}) - \rho_2(\boldsymbol{r}) \right\} \tag{24}$$

where n_0 is a smooth function on the real-space mesh and ρ_1, ρ_2 are true and smooth local terms defined only inside an atomic sphere. (For the case of several atoms per unit cell, the term in braces is replaced by a sum over the spheres.) If the local sphere density $\rho_1 - \rho_2$ has multipole moments q_M, the compensated mesh density is

$$\tilde{n}_0(\boldsymbol{r}) = n_0(\boldsymbol{r}) + \sum_M q_M G_M(\boldsymbol{r}) \tag{25}$$

where G_M is a gaussian of moment unity with angular momentum M, localized inside the muffin-tin sphere except for a negligible tail.

Similar to the other matrix elements, the potential energy integral can be written in the form

$$\int \tilde{F}_i^* V \tilde{F}_j \, d\boldsymbol{r} = \int F_i^* \tilde{V}_0 F_j \, d\boldsymbol{r} + \sum_{kk'LL'} C_{kL}^{(i)*} \pi_{kk'LL'} C_{k'L'}^{(j)} \ . \tag{26}$$

Again, the integral is first evaluated for the smooth mesh functions, after which the projection coefficients are combined with a small local matrix to add on the contribution of an atomic site. Here, the local potential matrix $\pi_{kk'LL'}$ is diagonal in L only if the sphere potential terms V_1 and $\tilde{V}_2$ are taken as spherical. To derive an expression for $\pi_{kk'LL'}$ we inspect the changes in the electrostatic and exchange-correlation energies due to a variation of the charge density. Presenting only the results, the final expression involves the multipole moments of $\tilde{P}_{kL}\tilde{P}_{k'L'} - P_{kL}P_{k'L'}$:

$$Q_{kk'LL'M} = \int_S \left\{ \tilde{P}_{kL}\tilde{P}_{k'L'} - P_{kL}P_{k'L'} \right\} r^m Y_M(\hat{r})\, d\boldsymbol{r} \ . \tag{27}$$

The matrix $\pi_{kk'LL'}$ turns out to be the sum of two contributions. The first term involves the smooth potential $\tilde{V}_0$ for the compensated mesh density:

$$\pi^{\text{mesh}}_{kk'LL'} = \sum_M Q_{kk'LL'M} \int \tilde{V}_0 G_M \, d\boldsymbol{r} \ . \tag{28}$$

The second term involves the true and smooth local potentials, V_1 and $\tilde{V}_2$:

$$\begin{aligned} \pi^{\text{local}}_{kk'LL'} = & \int_S \left\{ \tilde{P}_{kL} V_1 \tilde{P}_{k'L'} - P_{kL}\tilde{V}_2 P_{k'L'} \right\} d\boldsymbol{r} \\ & - \sum_M Q_{kk'LL'M} \int_S \tilde{V}_2 G_M \, d\boldsymbol{r} \ . \end{aligned} \tag{29}$$

Of course, 28 will cancel to a large extent against the last term in 29 since $\tilde{V}_2$ should be a local representation of the mesh potential $\tilde{V}_0$. It is necessary to include all the terms as described in order to minimize the total energy exactly.

These expressions have moved the situation quite a bit towards the desired environment-independence of all local atomic terms. In (29), the true potential V_1 is felt by the true partial density $\tilde{P}_{kL}\tilde{P}_{k'L'}$ while the smooth potential $\tilde{V}_2$ is felt by smooth partial density $P_{kL}P_{k'L'} + \sum Q_{kk'LL'M}G_M$. These two partial densities have the same multipole moments; this was essentially the definition of the quantity $Q_{kk'LL'M}$. If we modify the boundary conditions for the electrostatic potential inside the sphere in arbitrary way, this just adds the same linear combination of the harmonic functions $r^m Y_M(\boldsymbol{r})$ to both V_1 and $\tilde{V}_2$ (see below). It follows that the result of (29) does not depend on the electrostatic boundary conditions on the sphere, which can therefore be set to zero. The result is that (29) defines a quantity which can be calculated completely and unambiguously with only the density inside the sphere as input. However, this does not yet make $\pi^{\text{local}}_{kk'LL'}$ a fixed quantity when the $\tilde{P}_{kL}$ are kept frozen (as was the case for the overlap and kinetic energy matrix elements). The reason is that the local sphere density $\rho_1 - \rho_2$ can change in the course of a calculation, which will lead to changes in V_1 and $\tilde{V}_2$. Keeping the local sphere density frozen is thus an additional approximation, albeit reasonably plausible, which must be assumed in order to get full independence of π^{local} from the environment. While this was not done in the current method, further investigations in this direction would be interesting.

Finally, we discuss the significance of the term $\pi^{\text{mesh}}_{kk'LL'}$ given by (28). Augmentation modifies the charge density inside a muffin-tin sphere, including the total sphere charge as well as the higher multipole moments. In this sense our procedure is much more similar to Vanderbilt's ultrasmooth pseudopotential approach [6] than to the usual norm-conserving formulation. In the smooth representation of the problem, the sphere charge and the higher moments are mapped onto gaussians of the correct normalization. The term in (28) describes the interaction of these gaussians with the smooth mesh potential.

Construction of the Output Density

To complete the self-consistency loop, the output density must be constructed:

$$n^{\text{out}}(\boldsymbol{r}) = \sum_n w_n \, |\psi_n(\boldsymbol{r})|^2 \tag{30}$$

where the sum runs over the occupied eigenstates and the w_n are occupation numbers including spin degeneracy. Each wavefunction is a linear combination of the basis functions in the form

$$\psi_n(\boldsymbol{r}) = \sum_i T_{in} \tilde{F}_{in}(\boldsymbol{r}) \tag{31}$$

and the output density is a sum over the products $\tilde{F}^*_i \tilde{F}_j$:

$$n^{\text{out}}(\boldsymbol{r}) = \sum_{ij} \Big\{ \sum_n w_n T^*_{in} T_{jn} \Big\} \tilde{F}^*_i(\boldsymbol{r}) \tilde{F}_j(\boldsymbol{r}) \ . \tag{32}$$

The output density should be expressed in the same form as the input density in (24). That is, it should be given by a smooth mesh density n_0^{out} together with separate true and smooth local contributions $\rho_{1\nu}^{\text{out}}$ and $\rho_{2\nu}^{\text{out}}$ for each sphere ν.. In view of the preceding discussion of the augmentation process, the product of two augmented basis functions should be calculated as

$$\tilde{F}^*_i \tilde{F}_j = F^*_i F_j + \sum_{kk'LL'} C^{(i)*}_{kL} \Big\{ \tilde{P}_{kL} \tilde{P}_{k'L'} - P_{kL} P_{k'L'} \Big\} C^{(j)}_{k'L'} \tag{33}$$

where we have again assumed one atom per unit cell for notational simplicity. The integral over this quantity gave the overlap matrix, and the integral over this quantity times the potential gave the potential matrix element. In the latter case, the first term interacted with the smooth mesh potential $\tilde{V}_0$, the second with the local true potential V_1, and the third with the local smooth potential V_2 in the sphere. Correspondingly, the accumulated sums over the first, second, and third terms produce n_0^{out}, $\rho_{1\nu}^{\text{out}}$, and $\rho_{2\nu}^{\text{out}}$, respectively.

2.4 Representation of the Density and Potential

In the method presented here, some effort was taken to formulate matters such that low angular-momentum cutoffs can be used. As already mentioned above,

quantities defined throughout the crystal are represented as a smooth function which extend through the whole unit cell, plus contributions which are non-zero inside the muffin-tin spheres. This "additive augmentation" formulation has advantages over a piecewise definition, which would *replace* the smooth function by another quantity inside a sphere. It is the key to good accuracy at low angular-momentum cutoffs because it permits the smooth interstitial function to supply the higher angular momentum components.

To represent the valence density, we start with the smooth function $n_0(\boldsymbol{r})$ tabulated on the real-space mesh. For each atom ν we carry about a "true" density, which is to be added on, and a "smooth" contribution, which is to be subtracted and should equal the local expansion of $n_0(\boldsymbol{r})$ except for the angular-momentum cutoff. The potential is written in a similar way. Collecting together the corresponding expressions from above, we have

$$n(\boldsymbol{r}) = n_0(\boldsymbol{r}) + \sum_{\nu} \Big\{ \rho_{1\nu}(\boldsymbol{r}) - \rho_{2\nu}(\boldsymbol{r}) \Big\} \tag{34}$$

and

$$V(\boldsymbol{r}) = \tilde{V}_0(\boldsymbol{r}) + \sum_{\nu} \Big\{ V_{1\nu}(\boldsymbol{r}) - \tilde{V}_{2\nu}(\boldsymbol{r}) \Big\} \ . \tag{35}$$

Here $\rho_{1\nu}$ includes the core and the nucleus, and $\rho_{2\nu}$ includes their smooth "pseudo" versions, modeled by localized gaussians. Each local contribution $\rho_\nu = \rho_{1\nu} - \rho_{2\nu}$ is a sum over various angular momentum components, is non-zero only inside the corresponding MT sphere, and goes to zero smoothly as it approaches the MT radius $R^\nu_{\rm mt}$. As already emphasised, even if ρ_ν is truncated to a low angular momentum (possibly only to its spherical part) the full density $n(\boldsymbol{r})$ includes contributions for all L up to infinity. At high angular momentum, the radial part for any smooth function approaches a constant times r^l. It is pointless to include these components explicitly in the local representation, since they are already contained in $n_0(\boldsymbol{r})$.

A special situation arises if the core states are extended enough to spill out of the muffin-tin sphere. In such a case, the smooth core density is written as the sum of a gaussian and a single smooth Hankel function of angular momentum zero, whereby the latter term describes the spilled-out tail core density. In the "frozen overlapped core approximation" (FOCA) [16] the smooth crystal core density is obtained by overlapping these atomic contributions. This means that a further parameter enters, namely the smoothing radius which defines this core Hankel function. Whereas a large smoothing radius makes it possible to use a coarser real-space mesh to represent the overlapped core density, generally the correct core density outside the sphere can be modeled more accurately using a smaller value of the smoothing radius.

The potential is made by solving the Poisson equation for the input density and adding the exchange-correlation potential. This is described next.

Electrostatic Energy and Potential

At the start of each iteration, the crystal density is available in the form given in (34) above. To make the electrostatic potential, first a smooth "pseudodensity" is constructed which equals the given density in the interstitial region and has the correct multipole moments in all spheres. This is done by adding localized gaussians g_ν to the smooth mesh density with the same multipole moments as the local contributions $\rho_{1\nu} - \rho_{2\nu}$ within the spheres:

$$\tilde{n}_0 = n_0 + \sum_\nu g_\nu = n_0 + \sum_{\nu M} q_{\nu M} G_{\nu M} \tag{36}$$

The electrostatic potential of the smooth mesh density $n_0(\boldsymbol{r})$ is made by transforming to reciprocal space by fast Fourier transform, dividing the coefficients by the squares of the reciprocal vectors, and transforming back. The electrostatic potential due to the gaussian terms includes the contribution of the nuclei and is handled analytically in order to avoid the need for a higher plane wave cutoff. Together, this produces an electrostatic potential $\tilde{V}_0^{\mathrm{es}}(\boldsymbol{r})$ which is valid throughout the interstitial region and extends smoothly through the spheres.

Next, the electrostatic potential inside the spheres is determined. To recover the true density from the smooth pseudodensity, the following quantity must be added at each site ν:

$$\rho_{1\nu} - (\rho_{2\nu} + g_\nu) = \rho_{1\nu} - \tilde{\rho}_{2\nu} \ . \tag{37}$$

By construction, this local contribution has multipole moments which are zero. We solve the Poisson equation twice to obtain the "true" local potential $V_{1\nu}^{\mathrm{es}}$ and the "smooth" local potential $\tilde{V}_{2\nu}^{\mathrm{es}}$:

$$\Delta V_{1\nu}^{\mathrm{es}} = -8\pi\rho_{1\nu} \tag{38}$$

$$\Delta \tilde{V}_{2\nu}^{\mathrm{es}} = -8\pi(\rho_{2\nu} + g_\nu) \ . \tag{39}$$

The source terms $\rho_{1\nu}$ and $\tilde{\rho}_{2\nu} = \rho_{2\nu} + g_\nu$ have the same multipole moments, and we are really only interested in the difference $V_{1\nu}^{\mathrm{es}} - \tilde{V}_{2\nu}^{\mathrm{es}}$. Thus, the boundary conditions when solving the Poisson equation are here irrelevant, as long as the same set is used in both equations, and can be set to zero.

Finally, the electrostatic energy is obtained by adding together a smooth mesh term and local terms for all sites:

$$\int \tilde{n}_0(\boldsymbol{r}) \tilde{V}_0^{\mathrm{es}}(\boldsymbol{r})\, d\boldsymbol{r} + \sum_\nu \Big\{ \int_{S_\nu} \rho_{1\nu} V_{1\nu}^{\mathrm{es}}\, d\boldsymbol{r} - \int_{S_\nu} \tilde{\rho}_{2\nu} \tilde{V}_{2\nu}^{\mathrm{es}}\, d\boldsymbol{r} \Big\} \ . \tag{40}$$

As a general note on the energy integrals, expression (40) for the electrostatic energy involves an important convergence issue similar to the one discussed for the augmentation procedure. If Equation (34) for the density is taken seriously, it should be possible to add together $\rho_{1\nu}$ and $-\rho_{2\nu}$ for each site from the very beginning. However, in our approach the program explicitly carries about both functions in separate arrays, making it possible to evaluate the electrostatic

energy as described. In fact, the sum in (40) is not strictly the exact electrostatic energy for the density in (34) for any finite angular-momentum cutoff; again, a straightforward evaluation would lead to a large number of problematic cross terms.

In the description used here, there is a "true" and a "smooth" part to the problem which are kept separate. When evaluating energy integrals like the one above, the true density is not allowed to interact with the smooth potential and vice versa. The choice between the two possible expressions for an energy integral is only relevant for the rate of convergence with the angular-momentum cutoff, and not for the final outcome at convergence. When all angular-momentum components up to infinity are included, the distinction between the different ways to calculate the integral disappears. In the end, the main consequences of the formulation as in (40) are:

- In the resulting energy integrals, the higher angular momenta are supplied by the smooth density $n_0(\boldsymbol{r})$. That is, we start with an expression which contains all angular momentum components up to infinity in each sphere, then replace a few of the lower momentum terms.
- The aforementioned unwieldy cross terms do not have to be evaluated.
- The augmentation procedure described above cleanly separates into a smooth part plus local contributions, whereby each local term is independent of the environment of the atom.

Exchange-Correlation Energy and Potential

In the same spirit, the exchange-correlation energy is calculated by integrating a smooth function over the whole unit cell, then replacing the smooth contribution by the true one inside each MT sphere. Things are simpler here than for the electrostatic energy because no additional terms are needed to correct the multipole moments. Thus, the smooth exchange-correlation potential is made by evaluating it point-by-point for the smooth mesh density $n_0(\boldsymbol{r})$. Adding this to the electrostatic potential for the compensated density gives the total mesh potential

$$\tilde{V}_0(\boldsymbol{r}) = \tilde{V}_0^{\mathrm{es}}(\boldsymbol{r}) + \mu_{\mathrm{xc}}(n_0(\boldsymbol{r})) \tag{41}$$

Inside each sphere, two different exchange-correlation potentials are made and added respectively to the true and smooth local electrostatic potentials:

$$V_{1\nu}(\boldsymbol{r}) = V_{1\nu}^{\mathrm{es}}(\boldsymbol{r}) + \mu_{\mathrm{xc}}(\rho_{1\nu}(\boldsymbol{r})) \tag{42}$$

$$\tilde{V}_{2\nu}(\boldsymbol{r}) = \tilde{V}_{2\nu}^{\mathrm{es}}(\boldsymbol{r}) + \mu_{\mathrm{xc}}(\rho_{2\nu}(\boldsymbol{r})) \tag{43}$$

to produce the final potentials seen by the true and smooth densities at this site. The exchange-correlation energy is made by constructing the energy density ϵ_{xc} in exactly the same way and then adding together the smooth mesh term

$$\int n_0 \epsilon_{\mathrm{xc}}(n_0)\, d\boldsymbol{r} \tag{44}$$

and the sum over the local contributions

$$\int_{S_\nu} \rho_{1\nu}\epsilon_{\rm xc}(\rho_{1\nu})\,d\boldsymbol{r} - \int_{S_\nu} \rho_{2\nu}\epsilon_{\rm xc}(\rho_{2\nu})\,d\boldsymbol{r}\ . \tag{45}$$

Since $\epsilon_{\rm xc}(\rho)$ is a nonlinear function of the density, it mixes together all angular momentum components up to infinity. That is, $\epsilon_{\rm xc}(\rho_L + \rho_K)$ is not the same as $\epsilon_{\rm xc}(\rho_L) + \epsilon_{\rm xc}(\rho_K)$ and we should really include all L terms, even when making something as fundamental as the spherical part of $\epsilon_{\rm xc}(\rho)$. By evaluating the exchange-correlation energy as described, the interaction with the higher angular momenta is taken over by the smooth mesh contribution. When $\rho_{1\nu}$ and $\rho_{2\nu}$ are truncated to the same low angular momentum, the errors in the two integrands $\rho_{1\nu}\epsilon_{\rm xc}(\rho_{1\nu})$ and $\rho_{2\nu}\epsilon_{\rm xc}(\rho_{2\nu})$ are similar. Thus, while the two integrals in (45) converge rather sedately with the L cutoff separately, their difference converges rapidly.

Force Theorem

The force on an atom is defined as the negative gradient of the total energy respective to the corresponding atomic coordinates:

$$\boldsymbol{F}_\mu = -\nabla_\mu E_{\rm SC}(\boldsymbol{R}_1, \ldots, \boldsymbol{R}_\mu, \ldots, \boldsymbol{R}_N)\ . \tag{46}$$

Here $E_{\rm SC}$ is the full self-consistent total energy, which depends only on the atomic positions. In terms of small differences, the system is made self-consistent at two slightly different geometries and the total energies are compared. A force theorem is a closed expression, making it possible to calculate the forces $\boldsymbol{F}_\mu$ without explicitly shifting the atoms. Since the self-consistency process mixes together the various energy terms, a straightforward differentiation of the total energy expression is a strenuous (and not always feasible) way to obtain such a theorem.

A more convenient way to derive a force theorem is as follows [11]. Assume we want to calculate the forces at the geometry $\boldsymbol{P}^{(0)} = (\boldsymbol{R}_1^{(0)}, \ldots, \boldsymbol{R}_N^{(0)})$, for which the self-consistent density is known. For this purpose we make an arbitrary guess for the way in which the density responds as the atoms are moved. That is, we define a density $\tilde{n}_{\boldsymbol{P}}(\boldsymbol{r})$ for each geometry $\boldsymbol{P} = (\boldsymbol{R}_1, \ldots, \boldsymbol{R}_N)$ which conserves the total charge and which approaches the correct self-consistent density smoothly as $\boldsymbol{P} \to \boldsymbol{P}^{(0)}$. From the variational properties of the energy functional it follows that

$$\nabla_\mu E_{\rm SC}(\boldsymbol{R}_1, \ldots, \boldsymbol{R}_N) = \nabla_\mu \tilde{E}(\boldsymbol{R}_1, \ldots, \boldsymbol{R}_N) \tag{47}$$

where $\tilde{E}$ is defined as the Harris energy [17] evaluated for the guessed density:

$$\tilde{E}(\boldsymbol{R}_1, \ldots, \boldsymbol{R}_N) = E_{\rm H}[\tilde{n}_{\boldsymbol{P}}(\boldsymbol{r})]\ . \tag{48}$$

It follows that the forces can also be obtained by differentiating the auxiliary function $\tilde{E}$. This is a considerably easier task than differentiation of the self-consistent energy because the Harris energy can be written down explicitly as

function of the density. Furthermore, since the guessed function $\tilde{n}_{\boldsymbol{P}}(\boldsymbol{r})$ can be chosen freely, different force theorems can be obtained depending on this choice. Sensibly, $\tilde{n}_{\boldsymbol{P}}(\boldsymbol{r})$ should be defined in a way which makes it easy to perform the differentiation of $\tilde{E}$.

In the present formalism, the charge density is defined by a smooth mesh density $n_0(\boldsymbol{r})$ together with true and smooth local terms $\rho_{1\nu}(\boldsymbol{r})$ and $\rho_{2\nu}(\boldsymbol{r})$ associated with each site ν. If these functions represent the self-consistent density at geometry $\boldsymbol{P}^{(0)}$, a natural choice for the guessed density $\tilde{n}_{\boldsymbol{P}}(\boldsymbol{r})$ at a different geometry $\boldsymbol{P}$ is that $\rho_{1\nu}$ and $\rho_{2\nu}$ are carried along rigidly with the moving atoms while n_0 is unchanged.

This choice leads to a simple force theorem, as will be shown next. When the core states are treated separately, the Harris energy takes this form:

$$E_{\mathrm{H}} = \sum \epsilon_n^{\mathrm{val}} - \int n^{\mathrm{val}} V_{\mathrm{eff}} + U + E_{\mathrm{xc}} + \tilde{T}_{\mathrm{core}} \tag{49}$$

where $\tilde{T}_{\mathrm{core}}$ equals $\sum \epsilon_i^{\mathrm{core}} - \int n^{\mathrm{core}} V_{\mathrm{eff}}$ and all eigenvalues are calculated in the effective potential V_{eff}, made from the input density $n^{\mathrm{val}} + n^{\mathrm{core}}$. Integrals (including the implicit ones in U and E_{xc}) are all assembled in a similar way out of contributions from the smooth mesh density and from the spheres.

The aim is to derive the first-order change δE_{H} for the density change defined above. It reasonably straightforward that the last two terms give no contribution. Furthermore, all integrals over the spheres do not contribute. This is because the total-energy terms and the augmentation matrices for each atomic sphere are independent of the environment, depending only on the (here invariant) densities $\rho_{1\nu}$ and $\rho_{2\nu}$. On the other hand, a number of terms arise because the electrostatic potential on the mesh changes by some amount $\delta\tilde{V}_0$ as the compensating gaussians g_ν move along with the atoms. Each compensating gaussian g_ν can be split into a valence part g_ν^{val} and a smooth representation of the core and nucleus g_ν^{cn}. The compensated mesh density then equals

$$\tilde{n}_0 = n_0 + \sum_\nu g_\nu = \Big[n_0 + \sum_\nu g_\nu^{\mathrm{val}} \Big] + \sum_\nu g_\nu^{\mathrm{cn}} \tag{50}$$

where the term in brackets is the smooth representation of the valence density.

The contributions to δE_{H} from the first three terms of (49) are obtained as follows:

- By first-order perturbation theory, each eigenvalue $\epsilon_n^{\mathrm{val}}$ changes by

$$\delta\epsilon_n^{\mathrm{val}} = < C_n | \delta H - \epsilon_n^{\mathrm{val}} \delta S | C_n > \tag{51}$$

  where H and S are the Hamiltonian and overlap matrices and C_n is the column eigenvector. By summing over the occupied states and inspecting how $\tilde{V}_0$ enters into the Hamiltonian, the outcome is

$$\delta \sum \epsilon_n^{\mathrm{val}} = \int \delta\tilde{V}_0 \Big[n_0 + \sum_\nu g_\nu^{\mathrm{val}} \Big] + \delta^{\mathrm{R}} \sum \epsilon_n^{\mathrm{val}} \ . \tag{52}$$

Here δ^{R} refers to the eigenvalue change when the potential $\tilde{V}_0$ and the augmentation matrices entering into H and S are kept frozen.

- The change in the second term is

$$-\delta \int n^{\mathrm{val}} V_{\mathrm{eff}} = -\int \Big[n_0 + \sum_{\nu} g_{\nu}^{\mathrm{val}} \Big] \delta \tilde{V}_0 - \int \tilde{V}_0 \, \delta g_{\nu}^{\mathrm{val}} \ . \tag{53}$$

- The change in the third term is

$$\delta U = \int \tilde{V}_0 \Big[\delta g_{\nu}^{\mathrm{val}} + \delta g_{\nu}^{\mathrm{cn}} \Big] \ . \tag{54}$$

By summing these three contributions, the final force theorem is obtained:

$$\delta E_{\mathrm{H}} = \int \tilde{V}_0 \, \delta g_{\nu}^{\mathrm{cn}} + \delta^{\mathrm{R}} \sum \epsilon_n^{\mathrm{val}} \ . \tag{55}$$

Here the first term describes the force of the smooth density on the gaussian lumps which represent the core and the nucleus at each site. The second term is a generalized Pulay [18] term. It describes the eigenvalue shifts for a changing geometry but invariant smooth mesh potential and augmentation matrices. However, these augmentation matrices are used at the shifted atomic positions. This term can be evaluated in a straightforward manner since it mainly involves the gradients of the various quantities (such as the expansion coefficients of the envelope functions) which are needed to assemble the Hamiltonian and overlap matrices.

3 Tests of the Method

We have performed a number of tests to check the validity of the method. This we do in two ways. First, we investigate the sensitivity of the total energy to the various parameters at our disposal, i.e. the charge density and augmentation l-cutoffs l_ρ and l_a, the augmentation polynomial cutoff k_a, the smoothed density spacing, the treatment of the core, and the smoothing radii for the charge density, augmentation, and core, which we label respectively R^{ρ}_{sm}, R^{a}_{sm}, and R^{c}_{sm}. Second, we compare our results to other local-density calculations for several materials systems. Lastly, we present rules of thumb for the choice of basis.

3.1 Dependence on $l-$ and k-Cutoffs

Because the augmentation here shares a lot in common with a pseudopotential formulation, we expect that the l-cutoffs in the augmentation l_a and explicit representation of the charge density l_ρ to converge as efficiently. Indeed we find (see Fig. 3) that for l_a=2 the total energy is converged to $\sim 10^{-3}$ Ry/atom, and to $\sim 10^{-4}$ Ry/atom for l_a=3, even for the transition metal Ti. For a fixed l_a, a somewhat faster convergence in l_ρ was found: even l_ρ=0 was quite adequate

Table 1. Parameters for baseline reference in the tests for GaN, Ti, and Se. $R_{\rm mt}$, $R^c_{\rm sm}$ and $R^\rho_{\rm sm}$ are in units of the average Wigner-Seitz radius. As fractions of touching sphere radii, the $R_{\rm mt}$ are 0.99, 0.97, and 0.96, respectively

	$R_{\rm mt}$	$R^c_{\rm sm}$	$R^\rho_{\rm sm}$	k_a	l_a	l_ρ	mesh	basis
GaN	0.69	0.22	0.17	4	4	4	20	$spd \times 3$
(small basis)								$spd \times 2$
Ti	0.88	0.28	0.19	4	4	4	24	$spd \times 2{+}p$
(small basis)								$spd \times 2$
(minimal basis)								spd
Se	0.60	0.20	0.15	4	4	4	24	$spd \times 2{+}sp$

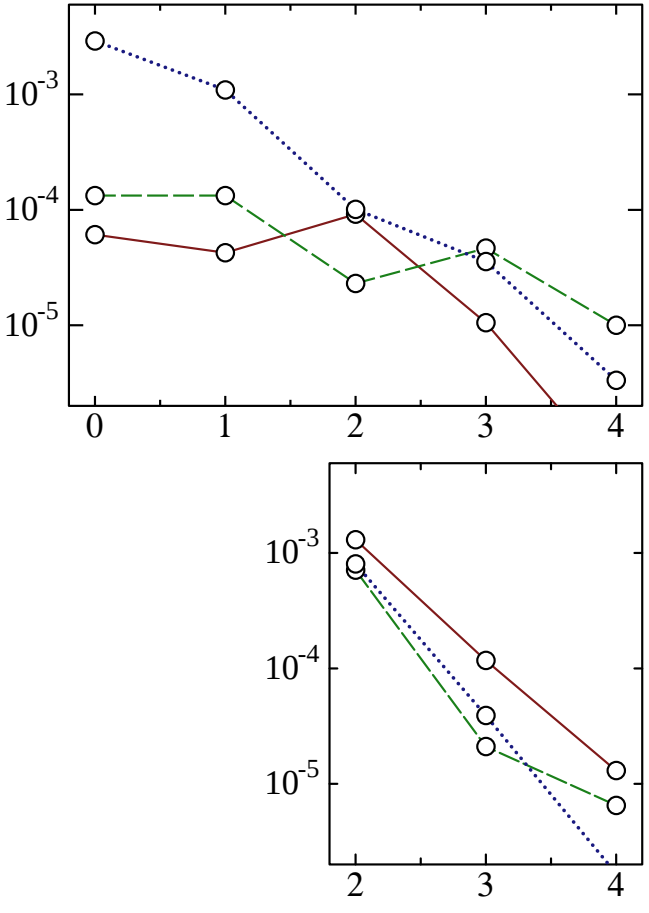

Fig. 3. Errors in the total energy, in Ry/atom, as a function of the l-cutoffs l_ρ for fixed l_a=5 (top panel) and l_a, with l_ρ=l_a (bottom panel). Solid line: GaN, dashed line: Ti; dotted line: Se.

for GaN and Ti, but this may be an artifact of the relatively high symmetry of those lattices.

The polynomial cutoff k_a in the P_{kl} expansion is another parameter whose convergence was checked. Because the tails have a rather weak energy dependence, we would expect that already after two terms (k_a=1) the total energy should be reasonable. Fig. 4 shows that the energy is converged to $\sim 10^{-3}$Ry/atom for k_a=1 (though the Ti calculation produced nonsensical results in that case), and $\sim 10^{-4}$Ry/atom for k_a=2. It is evident that the convergence of k_a will be sensitive to the augmentation smoothing $R^a_{\rm sm}$, i.e. the smoothing radius for which one projects tails of the envelope functions into polynomials inside the augmentation site. The larger one makes $R^a_{\rm sm}$, the more broadly dispersed the errors in the polynomial expansion; the optimal choice of $R^a_{\rm sm}$ distributes the errors most evenly throughout the augmentation sphere. From experience we have found that $R^a_{\rm sm} \sim R_{\rm mt}/3$ is approximately the smoothing for which the most rapid convergence with k_a is attained.

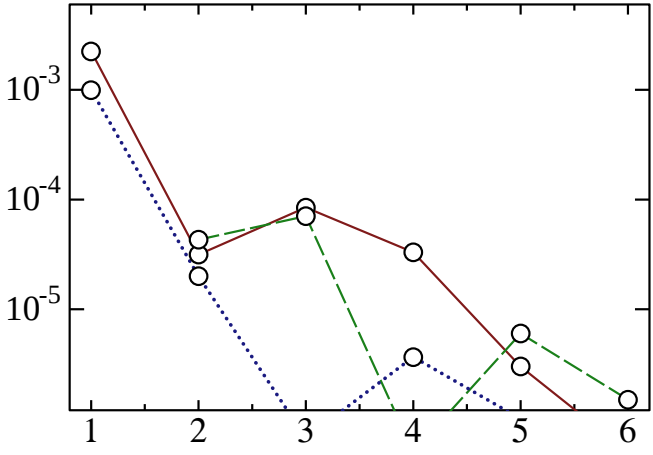

Fig. 4. Errors in the total energy, in Ry/atom, as a function of the k-cutoff. Solid line: GaN, dashed line: Ti; dotted line: Se.

3.2 Dependence on MT and Smoothing Radii

One critical test of the theory's validity is its dependence of the total energy on muffin-tin radius $R_{\rm mt}$, because by changing $R_{\rm mt}$ one changes the representation of the basis. If the basis is complete, and all the cutoffs (l_a, l_ρ, k_a and mesh spacing) and smoothing radii ($R^c_{\rm sm}$, $R^\rho_{\rm sm}$) are set fine enough, there should be no dependence on $R_{\rm mt}$. Indeed, we find this to be essentially true for the cases we studied (ZB GaN, Se, and Ti). Parameters for which the sensitivity was checked in the greatest detail were the core smoothing radius $R^c_{\rm sm}$, and truncation of the basis. Using the reference parameters in Table 1, the total energy was found to

be constant for all three tests to within ∼1 mRy/atom when the MT radius was varied from ∼0.85×R_T, to ∼1.1×R_T, where R_T is the touching-sphere radius. Fig. 5 illustrates the dependence for GaN and Ti, for both the baseline case and when one parameter was changed relative to it.

That the energy is independent of $R_{\rm mt}$ for $R_{\rm mt} < R_T$ is a demonstration that the errors can be well controlled, and the energy converged to a high precision as with the LAPW technique. That the energy is is independent of $R_{\rm mt}$ for $R_{\rm mt} > R_T$ is less obvious, since spheres overlap and wave functions have different, and inconsistent representations. Previous implementations of full-potential, augmented-wave programs do not show this independence, and we attribute this to the fact that both the augmentation and the local contributions to the potential go smoothly and differentiably to zero at the MT boundary; thus the overlapping regions are "doubly counted" with a very small weight.

Fig. 5 shows that the energy is rather sensitive to the core smoothing radius. This is not surprising, since the core energy is very large and small changes in the core density can produce significant effects. But, energy differences between different structures should be significantly smaller than this. Also, as expected, there is a much stronger dependence on the total energy when the basis is made small. (This error can be reduced by re-optimizing the wave function parameters for each new choice of MT radius. No attempt was made to do this.) As one shrinks $R_{\rm mt}$, the interstitial volume increases and throws greater weight into the interstitial representation. The figure also shows that $R^{\rho}_{\rm sm}$ must be small enough to really properly confine the projection of the MT potential into the augmentation sphere, or about 0.25×$R_{\rm mt}$. $R^{c}_{\rm sm}$ can be set set to about 0.4×$R_{\rm mt}$, negligible loss in accuracy, and up to about 0.6×$R_{\rm mt}$, with a loss in absolute accuracy of ∼1 mRy/atom, provided $R_{\rm mt}$ is kept close to touching. This is quite adequate for most applications, since such error will cancel when comparing relative energy differences. Some information about the MT dependence in Se is discussed in the comparison to other LDA results.

3.3 Dependence of the Total Energy on Basis

Having the extra degrees of freedom in the basis is one key advantage the present scheme has over conventional LMTO approaches. The two degrees of freedom, the energy ϵ and smoothing radius $R_{\rm sm}$ can be adjusted for each orbital. As we show here, a minimal basis of *spd* orbitals produces ground state energies within a few mRy of the completely converged LDA energy in close-packed systems; similar convergence can be achieved with an *spdsp* basis in open structures.

As of yet, there is no automatic prescription for finding the optimum choice of these parameters suitable to the solid, and we offer some general rules of thumb based on practical experience. One obvious choice is to determine $R_{\rm sm}$ and ϵ from the free-atomic wave functions. This turns to be a reasonable choice, particularly for the compact orbitals such as transition metal d orbitals or deep states such as the Ga d semicore levels.

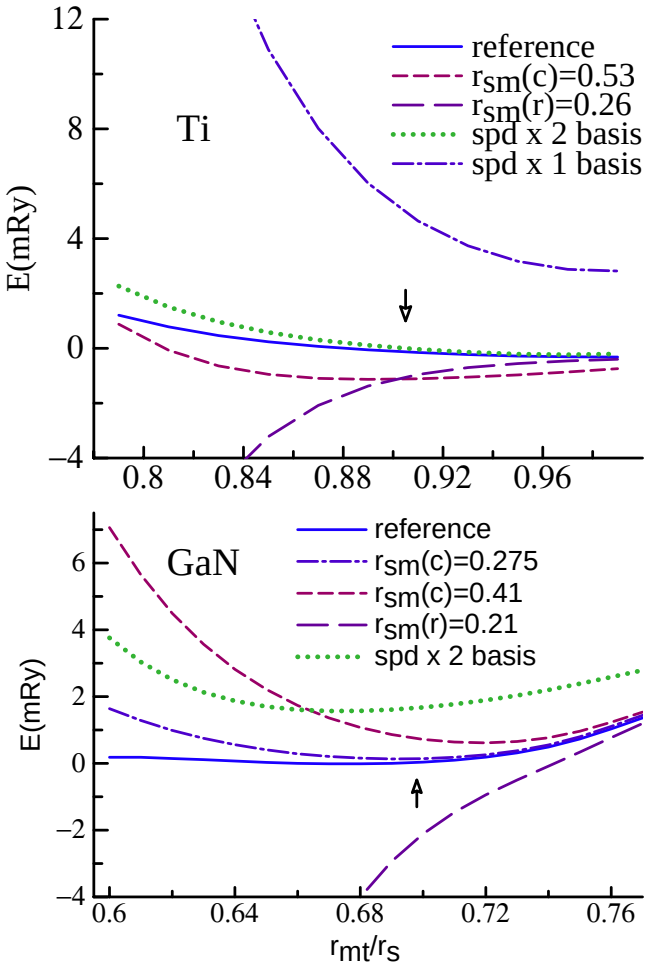

Fig. 5. Dependence of the total energy, in Ry/atom on muffin-tin radius. Reference parameters are provided in Table 1. Top: Ti; bottom: ZB GaN. Arrows mark MT radius for touching spheres. The large $R^c_{\rm sm}$ (short dashed line) correspond to $R^c_{\rm sm}{\sim}0.6{\times}R_T$; the reference $R^c_{\rm sm}$ (solid lines) correspond to ${\sim}0.32{\times}R_T$. The large $R^\rho_{\rm sm}$ (long dashed line) correspond to $R^\rho_{\rm sm}{\sim}0.3{\times}R_T$; the reference $R^\rho_{\rm sm}$ correspond to $R^\rho_{\rm sm}$ ${\sim}0.25{\times}R_T$. Calculations repeated using the perturbation approach to the core-valence interaction are indistinguishable from the ones shown.

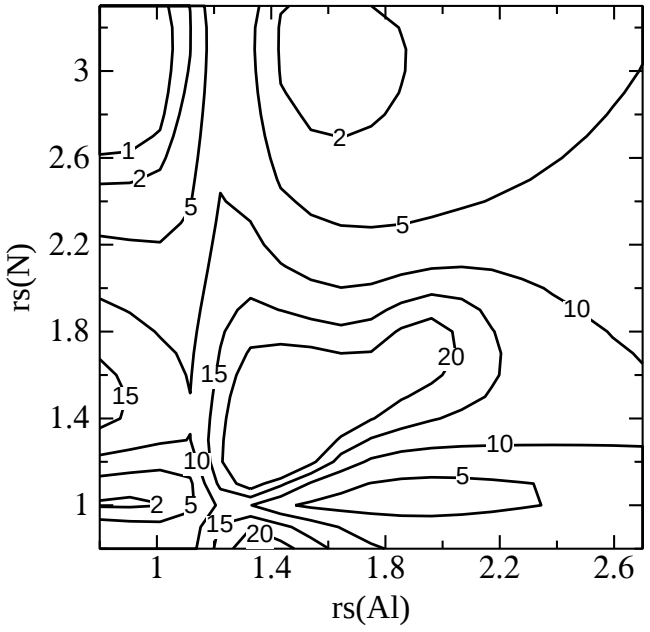

Fig. 6. Contours of the deviation of the total energy from the optimum value, in mRy/cell, as functions of $R_{\rm sm}$ for Al and N. All the orbitals on each atom were given the same $R_{\rm sm}$. There are four minima, at ($R_{\rm sm}$(Al),$R_{\rm sm}$(N))$\approx$ (0.95,1), (0.85,3), (1.9,1), and (1.6,3). All the minima are within 4 mRy of each other.

Interestingly, the extended *sp* orbitals usually have two very different optimum values of $R_{\rm sm}$. This is illustrated for AlN in Fig. 6. Some rules of thumb, gathered from experience for a number of cases, are:

- For localized, narrow-band orbitals, the values of $R_{\rm sm}$ and ϵ fit to the free atom are close to optimum.
- Reasonable choices of ϵ are $-1 < \epsilon < 0$. For wide-band orbitals, the best choice of ϵ is near zero.
- For *sp* orbitals, the "small" optimum $R_{\rm sm}$ is usually $\approx$2/3 $R_{\rm mt}$. The "large" optimum $R_{\rm sm}$ is $\approx$1.5 $R_{\rm mt}$ and mostly resembles a gaussian orbital in the near $R_{\rm mt}$.
- For close-packed structures, a minimal basis consisting of the nine *spd* orbitals (16 for rare earths) is sufficient to produce a total energy with $\sim$5mRy/atom or so of the totally converged LDA result. The error is slightly larger for heavier elements, unless *f* orbitals are included.
- For open structures, a basis consisting of thirteen *spdsp* orbitals usually produces a result with a similar accuracy. In that case, choosing one set of *sp* orbitals with a "small" $R_{\rm sm}$, and the the other with a large $R_{\rm sm}$ seems to work well. There is an occasional exception to this rule; for example, the deep Ga *d* states in GaN require two sets of *d* orbitals to reach this accuracy.

- The fastest convergence in k_a was achieved for $R^a_{\rm sm}$, is $\sim 1/3 \times R_{\rm mt}$; using that value, k_a=2 or 3 was adequate for all systems we studied.

3.4 Comparison with Other Density-Functional Calculations

First, we investigate the cases of elemental Se and Te. These form an open, low-symmetry crystal with approximately 90-degree bond angles. The electronic structure is approximately described by pure atomic p orbitals linked together in one-dimensional chains, with a strong σ bond connecting neighbors in the chain and with a weak interaction between the chains. The weak inter-chain interaction combined σ-like character of the bond make the stiffness of the crystal weak with respect to angular distortions, and thus pose a rather stringent test for the local-density approximation, and the low symmetry and open structure make a a good test for an atom-centered method's method's ability to reproduce the converged local-density result. The crystal structure of Se and Te is hexagonal with three atoms per unit cell, and may be specified by the a and c parameters of the hexagonal cell, and one internal displacement parameter u. Using a plane-wave pseudopotential approach, Dal Corso and Resta[19] have calculated the bonding in some detail, and they have also calculated the equilibrium structure of Se for both the LDA and adding gradient corrections.

Table 2 shows our LDA structures agrees well with that of Corso and Resta. For both calculations, the LDA predicts reasonably well the strong intra-chain bond length, but rather poorly the inter-chain bond length. The table also shows the dependence of the structural parameters and total energy on the size of basis and the MT radius. The reference basis consisted of one *spd* group with $R_{\rm sm}$=1.3, ϵ=-0.1 Ry and an additional *sp* group with $R_{\rm sm}$=1.4, ϵ=-1 Ry, for 13 orbitals. Adding a second d and a third s orbital lowers the energy by 2/3 mRy per atom; adding an f orbital lowers the energy by an additional 2.5 mRy per atom. Thus, the 13-orbitals basis comes to within $\sim$ 3 mRy/atom of a totally converged energy. Also, the table illustrates the dependence on R_{MT}: the lattice parameters vary weakly and the total energy varies by $\sim$1 mRy/atom when R_{MT} is changed from -10 to 10 percent of touching for the minimal basis; the dependence is slightly weaker with a large basis.

Next, we examine in some detail the behavior of the (Al,Ga,In)N compounds, because it involves several useful tests of the method's validity. The deep Ga and In d levels must be included in the valence for a well-converged calculation. (Pseudopotential results that pseudize the d electrons differ considerably from those that do not.) Even though the states are deep, it turns out that they must treated carefully. For example, to produce accurate heats of mixing of the GaInN alloy it was found that two sets of Ga and In d orbitals were required.

Our next case concerns the [111] γ-surface of Ni. The [111] glide planes are connected with dislocation motion, and therefore are of significant practical interest. To model the γ surface with the periodic boundary conditions necessitated by the present computational approach, we employ a supercell of 8 [111] planes of Ni atoms, with the fault between the fourth and fifth planes. The first and 8th layers were separated by a vacuum of two layers. Lattice vectors in the plane of

Table 2. Crystal structure properties of Se. Lattice parameters a and c are in atomic units, as are intrachain bond length d_1 and interchain bond length d_2; u is an internal displacement parameter as described in Ref. [19] and E is the binding energy relative to the free atom, in Ry

	a	c	u	d_1	d_2	E
[a], $R_{\rm mt}$=2.11	7.45	9.64	0.258	4.63	5.83	-0.7121
[a], $R_{\rm mt}$=2.32	7.40	9.57	0.266	4.67	5.75	-0.7147
[a], $R_{\rm mt}$=2.45	7.40	9.57	0.267	4.68	5.73	-0.7152
[a], $R_{\rm mt}$=2.58	7.40	9.59	0.268	4.69	5.72	-0.7149
[b], $R_{\rm mt}$=2.11	7.40	9.58	0.259	4.61	5.78	-0.7152
[b], $R_{\rm mt}$=2.32	7.41	9.61	0.264	4.66	5.76	-0.7167
[c], $R_{\rm mt}$=2.32	7.42	9.57	0.264	4.67	5.77	-0.7261
[d], $R_{\rm mt}$=2.32	7.38	9.60	0.270	4.71	5.70	-0.7131
[e], $R_{\rm mt}$=2.32	7.40	9.59	0.267	4.72	5.72	-0.7131
Ref. [19]	7.45	9.68	0.256	4.61	5.84	
Experiment	8.23	9.37	0.228	4.51	6.45	

[a] 13 orbital basis
[b] 21 orbital basis
[c] 21+f orbital basis
[d] l_ρ=0
[e] l_a=2 l_ρ=2

the fault were $[1\bar{1}0]$ and $[11\bar{2}]$, so that each layer had two atoms. The total energy was calculated as a function of the translation τ along $[11\bar{2}]$. It was assumed that the four layers separating the fault and the vacuum was large enough that there was no coupling between the fault and the surface. The thickness of the vacuum itself was checked and the energy shown in Fig. 7 change was negligible when the vacuum thickness was doubled. l_a and l_ρ were taken to be 3, $R^c_{\rm sm}$ to be $0.4\times R_{\rm mt}$.

Fig. 7 shows the energy of the Ni γ surface, without allowing any atomic relaxation. It was calculated using a 9-orbital minimal basis of *spd* orbitals of energy -0.1 Ry and smoothing radius $R_{\rm sm}$ 2.0 a.u. and 1.0 a.u. for *sp* and *d* orbitals, respectively (dark circles), and then repeated for a basis enlarged by an *spd* set of energy -1 Ry, $R_{\rm sm}$=1.3 a.u. (light circles). As the Figure shows, the addition of the larger basis made a 5% correction to the barrier. The BZ was integrated by sampling, using 27 irreducible points. A conservative mesh of $15\times24\times120$ divisions was used, corresponding to a mesh spacing of $\sim$0.31 a.u.; the inset in Fig. 7 shows the error in the barrier as a function of the mesh spacing. It is seen that an acceptable error was obtained for a mesh spacing of $\sim$0.5 a.u.. This corresponds to an error in the numerical integration of kinetic energy of $\sim 10^{-6}$ Ry.

Table 3. Lattice properties of III-nitrides. Lattice constant a is in Å. All data are for the wurtzite structure, except for rows marked a (ZB). Data marked OLD-FP are calculations from the present work, using the LDA and the exchange-correlation functional of Barth and Hedin [34]. Data marked GGA-LMTO employ gradient-corrected functional of Perdew [35]. Data marked PWPP are LDA results using a plane-wave basis and a pseudopotential with the Ga 3d and In 4d in the valence [33]. $\Delta E_{\mathrm{ZB-WZ}}$ is the ZB-WZ energy difference per atom pair, in meV

		AlN	GaN	InN
Small basis	a	3.096	3.163	3.525
	c/a	1.600	1.629	1.606
	u	0.3818	0.3775	0.3805
	a (ZB)	4.353	4.481	4.961
	$\Delta E_{\mathrm{ZB-WZ}}$	54	14	23
Large basis	a	3.095	3.160	3.509
	c/a	1.601	1.629	1.613
	u	0.3818	0.3766	0.3794
	a (ZB)		4.478	4.947
	$\Delta E_{\mathrm{ZB-WZ}}$	51	12	18
Old-FPLMTO	a	3.091	3.160	3.528
	c/a	1.602	1.626	1.611
	u	0.381	0.377	0.380
	a (ZB)	4.345	4.464	4.957
LAPW[h]	a	3.098	3.170	3.546
	c/a	1.601	1.625	1.612
	u	0.382	0.377	0.379
	a (ZB)	4.355	4.476	4.964
	$\Delta E_{\mathrm{ZB-WZ}}$	45	11	21
PWPP[f]	a	3.084	3.162	3.501
	c/a	1.604	1.626	1.619
	u	0.381	0.377	0.378
	a (ZB)	4.342	4.460	4.932
	$\Delta E_{\mathrm{ZB-WZ}}$	36	22	20
Experiment	a	3.11[d]	3.190[d]	3.544[e]
	c/a	1.601[d]	1.626[d]	1.613[e]
	u	0.382[d]	0.377[d]	
	a (ZB)	4.38 [a]	4.52-4.55[b]	4.98[c]

[a] Ref. [24]
[b] Refs. [25–29], taken from Ref. [23]
[c] Ref. [22]
[d] Ref. [30]
[e] Ref. [21]
[f] Structural properties taken from Ref. [33]; $\Delta E_{\mathrm{ZB-WZ}}$ taken from Ref. [20].
[g] Taken from Ref. [31]
[h] Taken from Ref. [32]

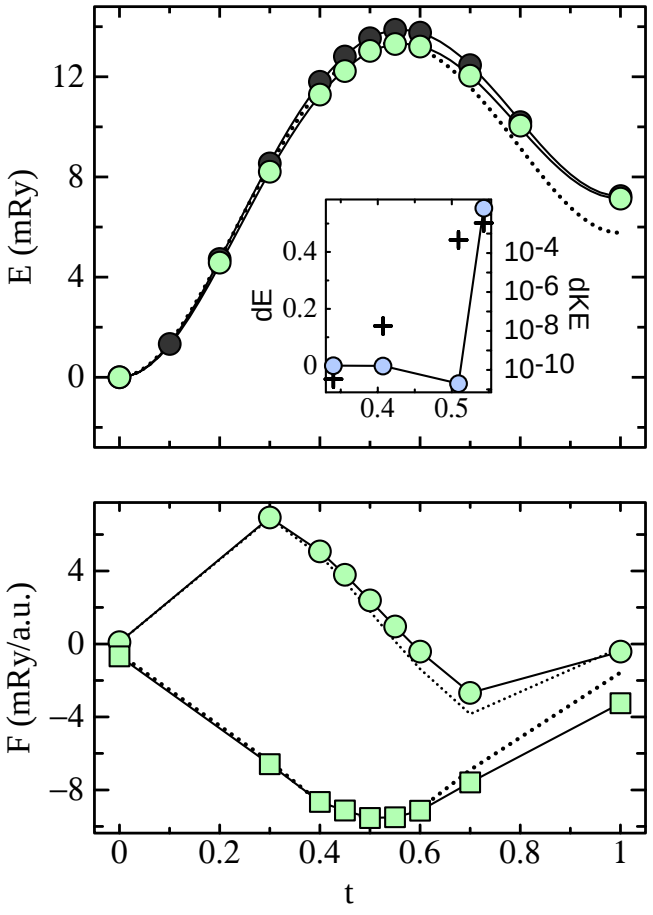

Fig. 7. The total energy for a γ surface of [111] Ni, as as function of translation $\tau/4[11\bar{2}]$, as described in the text. Upper panel: total energy (mRy/unit cell) for a nine-orbital basis (dark circles), an 18-orbital basis (light circles) and for a pseudopotential calculation (dotted line), using VASP. Inset: circles show error in the peak energy (mRy) as a function of mesh spacing in a.u.. Crosses show corresponding error in numerical integration of the kinetic energy of the d orbital on the mesh. Lower panel: x (circles) and y (squares) force on the atoms at the interface. Dotted lines show VASP result.

These results were compared to a pseudopotential calculation using Vanderbilt's [6] ultrasoft potentials; this latter calculation was performed with the VASP code [36]. The VASP code used the same BZ integration, and the default mesh (16×24×108 divisions). Those results are illustrated by the dotted lines in Fig. 7. There is good agreement with VASP throughout except for a modest discrepancy for $\tau \sim 1$. The source of the discrepancy is not clear; it would seem that in the all-electron case, the remaining sources of error (truncation in basis, truncation in l, smoothing of the core) all appear to be controlled.

4 Summary

In this paper, we have presented a newly developed full-potential LMTO method with the following properties:

- The potential is treated without any shape approximation, based on a muffin-tin type of geometry consisting of non-overlapping atomic spheres and an interstitial region.
- Empty spheres are not needed for any system.
- The results can be systematically improved by increasing the convergence parameters.
- The forces are as accurate derivatives of the total energy.

Similar to some previous FP-LMTO approaches, the interstitial density and potential are represented on a real-space mesh while the wavefunctions are assembled from atom-centered basis functions with well-defined angular momenta. In order to reduce the basis size further and to make the evaluation of integrals more efficient, we have introduced a new type of function which plays the role of the smooth envelope. These "smooth Hankel functions" are analytic in all parts of space and equal the standard Hankel functions at large radii. Closer to the origin, they bend over smoothly and are nonsingular. To introduce atomic detail into these envelope functions, a modified augmentation scheme was employed which combines some features of the projector-augmented wave method and the pseudopotential approach. By systematically using additive augmentation for the density, the potential, and the wavefunctions, the approach allows low angular momentum cutoffs throughout. Tests were performed to assess the quality of the method. Results have shown that state-of-the-art convergence can indeed be attained with low angular momentum cutoffs and small basis sets. Since the forces are calculated and the potential is treated without any shape approximation, the method presented here can be used to relax atomic structures and to study the energy changes associated with perturbations of the atoms around their equilibrium sites.

References

1. O.K. Andersen, Phys. Rev. B **12**, 3060 (1975).
2. P. Hohenberg and W. Kohn, Phys. Rev. **136**, B6864 (1964); W. Kohn and L.J. Sham, Phys. Rev. **140**, A1133 (1965); R.O. Jones and O. Gunnarsson, Rev. Mod. Phys. **61**, 689 (1989).
3. D. Glötzel, B. Segall, and O.K. Andersen, Solid State Commun. **36**, 403 (1980); A.K. McMahan, Phys. Rev. B **30**, 5835 (1984).
4. R. Car and M. Parrinello, Phys. Rev. Lett. **55**, 2471 (1985).
5. P.E. Blöchl, Phys. Rev. B **50**, 17 953 (1994).
6. D. Vanderbilt, Phys. Rev. B **41**, 7892 (1990).
7. K.H. Weyrich, Phys. Rev. B **37**, 10269 (1988).
8. J. Wills, unpublished.
9. S.Y. Savrasov, Phys. Rev. B **54**, 16470 (1996).

10. M. Methfessel, Phys. Rev. B **38**, 1537 (1988); M. Methfessel, C.O. Rodriguez, and O.K. Andersen, Phys. Rev. B **40**, 2009 (1989).
11. M. Methfessel and M. van Schilfgaarde, Phys. Rev. B **48**, 4937 (1993).
12. M. Springborg and O.K. Andersen, J. Chem. Phys. **87**, 7125 (1987).
13. M. Methfessel, PhD thesis, Katholieke Universiteit Nijmegen (1986).
14. E. Bott, Diplomarbeit, Technical University Darmstadt (1997); E. Bott, M. Methfessel, W. Krabs, and P.C. Schmidt, J. Math. Phys. **39**, 3393 (1998).
15. G.B. Bachelet, D.R. Haman, and M. Schlüter, Phys. Rev. B **26**, 4199 (1982).
16. M. Methfessel, *NFP Manual* (Institute for Semiconductor Physics, Frankfurt (Oder), 1997).
17. J. Harris, Phys. Rev. B **31**, 1770 (1985); W.M.C. Foulkes and R. Haydock, Phys. Rev. B **39**, 12 520 (1989).
18. P. Pulay, Mol. Phys. **17**, 197 (1969).
19. A. Dal Corso and R. Resta, Phys. Rev. B**50**, 4327 (1994).
20. C.-Y. Yeh, Z. W. Lu, S. Froyen and A. Zunger, Phys. Rev. B**46**, 10086 (1992).
21. K. Osamura, S. Naka and Y. Murakami, J. Appl. Phys. **46**, 3432 (1975).
22. S. Strite, D. Chandrasekhar, D. J. Smith, J. Sariel, N. Teraguchi and H. Morkoç, J. Crys. Growth **127**, 204 (1993).
23. H. Morkoç, S. Strite, G. B. Gao, M. E. Lin, B. Sverdlov and M. Burns, J. Appl. Phys. **76**, 1363 (1994).
24. P. Petrov, E. Mojab, R. C. Powell and J. E. Greene Appl. Phys. Lett. **60** 2491 (1992).
25. M. J. Paisley, Z. Sitar, J. B. Posthill and R. F. Davis, J. Vac. Sci. Technol. A**7** 1701 (1989).
26. S. Strite, J. Ruan, Z. Li, A. Salvador, H. Chen D. J. Smith, W. Y. Choyke and H. Morkoç, J. Vac. Sci. Technol. B **9**, 1924 (1991).
27. R. C. Powell, G. A. Tomasch, Y.-W. Kim, J. A. Thornton and J. E. Green, Mater. Res. Soc. Symp. Proc. **162**, 525 (1990).
28. T. Lei, M. Fanciulli, R. J. Molnar, T. D. Moustakas, R. J. Graham and J. Scanlon, Appl. Phys. Lett. **59**, 944 (1991).
29. M. Mizuta, S. Fujieda, Y. Matsumoto and T. Kawamura, Jpn. J. Appl. Phys. **25**, L945 (1986).
30. H. Schulz and K. H. Thiemann, Sol. State Commun. **23**, 815 (1977).
31. M. van Schilfgaarde, A. Sher and A.-B. Chen "Theory of AlN, GaN, InN and Their Alloys," J. Crystal Growth **178**, 8 (1997).
32. S.- H.- Wei, private communication.
33. A. F. Wright and J. S. Nelson, Phys. Rev. B**51**, 7866 (1995); A. F. Wright and J. S. Nelson, Phys. Rev. B**50**, 2159 (1994).
34. U. von Barth and L. Hedin, J. Phys. C**5**, 1629 (1972).
35. J. P. Perdew, K. Burke, and M. Ernzerhof, Phys. Rev. Lett. **77**, 3865 (1996).
36. G. Kresse and J. Hafner, Phys. Rev. B**47**, 558 (1993); G. Kresse, Thesis, Technische Universität Wien 1993; G. Kresse and J. Furthmüller, Comput. Mat. Sci. 6, 15-50 (1996); G. Kresse and J. Furthmüller, Phys. Rev. B**54**, 11169 (1996).